Strain effects of missing dimer defects on dimer buckling of the Si(100) surface

Masakuni Okamoto* and Takashi Yokoyama
Takayanagi Particle Surface Project, ERATO, Japan Science and Technology Corporation, 4-1-8 Honcho, Kawaguchi, Saitama 332-0012, Japan

Tsuyoshi Uda
Joint Research Center for Atom Technology (JRCAT)-Angstrom Technology Partnership (ATP), 1-1-4 Higashi, Tsukuba, Ibaraki 305-0046, Japan

Kunio Takayanagi
Department of Material Science and Engineering, Tokyo Institute of Technology, 4259 Nagatsuta, Midori-ku, Yokohama 226-8502, Japan

(Received 19 June 2000)

We observed a characteristic dimer buckling pattern around a missing dimer defect on the Si(100) surface near the critical temperature by low-temperature scanning tunneling microscopy (STM). We studied the dynamical properties of this surface by using a Monte Carlo technique on the model Ising system, regarding the buckled dimers as Ising spins. We determined the interaction parameters by the *ab initio* calculations within local-density approximation. The simulated STM images were in good agreement with the observed images in the whole temperature range.

I. INTRODUCTION

The Si(100) surface is very important for silicon devices because of its smaller surface/interface trap state density[1] and higher mobility[2] than any other surface orientations. Extensive studies, both theoretical[3–8] and experimental,[9–11] have been made. They have revealed that the Si(100) surface consists of buckled dimers. The dimers are oscillating thermally with period of about 200 fs (Ref. 12) near room temperature. When this surface is observed by the scanning tunneling microscopy (STM) having typical measurement period of about 0.1 s, an averaged image of 2×1 periodicity is observed. The order-disorder phase change takes place at 200 K ($\approx T_c^{exp}$),[9,10] and the surface is frozen into the $c(4\times2)$ structure,[11] where the buckling alternates perpendicular to as well as along the dimer row.

The Si(100) surface contains several defects. They are classified into three groups; type-A, type-B, and type-C defects.[13] While the type-A and the type-B defects are well identified as a single-dimer vacancy,[14] and a double-dimer vacancy, respectively, the atomic structure of the type-C defect is still in controversy.[15–17] Almost all type-B and type-C defects disappeared and only type-A defects remained for the surface of defect density less than 1%.[18] This is consistent with the theoretical result by Pandey[14] that the type-A defects are electronically stable. It should be noted that the type-C defects induce the dimer buckling even at room temperature.[13] On the other hand, the type-A and the type-B defects have never been observed to affect the buckling at room temperature.[13]

Very recently, however, we observed that the type-A defects induced characteristic buckling patterns near T_c^{exp} by using the detailed low-temperature STM;[18] (i) When $T \gg T_c^{exp}$, the (2×1) reconstruction was observed in the whole area. (ii) When $T \approx T_c^{exp}$, the dimer row with a type-A defect was still symmetric, while the neighboring two dimer rows were buckled. The buckling was pinned such that the atoms adjacent to the type-A defects were protruded. (iii) Well below T_c^{exp}, the $c(4\times2)$ reconstruction was observed in the whole area. In the previous papers,[18,19] we have shown that the above phenomena might be explained qualitatively by introducing the strain energy caused by the type-A defect. However, the strain energy A defined in Ref. 19 [and the same definition is used in Eq. (1) of the present paper] was only a fitting parameter, and a subtle discrepancy between the experiment and the theory at the vicinity of the critical temperature was remained unsolved.

In the present paper, we determine the strain parameter A by using reliable *ab initio* calculations and perform a detailed Monte Carlo simulation with about ten times greater Monte Carlo steps (MCS) than that of the previous one in order to derive reliable results even at the critical temperature.

II. STRAIN ENERGY

A. Model and method

The dynamical properties of the Si(100) surface has been investigated successfully on the Ising model, where the buckled dimers are regarded as Ising spins.[20] The arrows on the buckled dimers in Fig. 1 correspond to spin directions ($\sigma=\pm1$). The spins were located on the square lattice and the interactions between Ising spins V, H, and D and are illustrated in Fig. 2. We also introduced in Fig. 2 the strain energy parameter A, which pins the directions of two spins adjacent to a missing ‘‘spin.’’ The physical meaning and the value of A will be discussed detail in the next section. The Hamiltonian $\mathcal{H}$ of this Ising model is as follows:

 ©2000 The American Physical Society

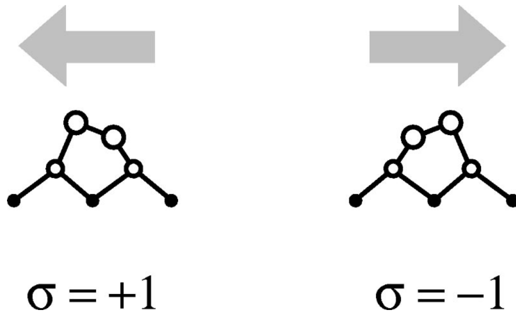

FIG. 1. Correspondence between dimer and spin.

$$\mathcal{H}=-V\sum_{\langle i,j\rangle}\sigma_{i,j}\sigma_{i,j+1}-H\sum_{\langle i,j\rangle}\sigma_{i,j}\sigma_{i+1,j}-D\sum_{\langle i,j\rangle}\sigma_{i,j}(\sigma_{i+1,j+1}+\sigma_{i+1,j-1})-A\sum_{\langle i_d,j_d\rangle}(\sigma_{i_d+1,j_d}-\sigma_{i_d-1,j_d}), \quad (1)$$

where positions of the type-A defects are denoted by (i_d,j_d), and $\langle i,j\rangle$ indicates the set of corresponding sites i and j.

In order to determine the interaction parameters, we have calculated total energies of clean surface and of the surface with the type-A defect for several buckling configurations. We used clusters consisting of four layers and nine dimers for clean surface and eight dimers for the surface with a type-A defect. The dangling bonds of the subsurface layers are terminated by the hydrogen atoms.

B. *Ab initio* calculation

Our *ab initio* calculation was based on the local-density-functional approach. In the calculation, frozen core approximation, localized numerical basis functions of the 6-31G^{**} level and exchange-correlation functional of Vosko, Wilk, and Nusair[21] were used. Hydrogen atoms were fixed during structure optimization.

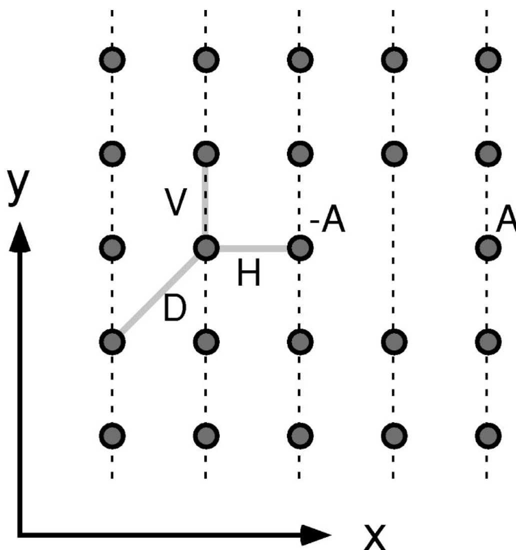

FIG. 2. Definition of interaction parameters V, H, D, and A for the Ising model.

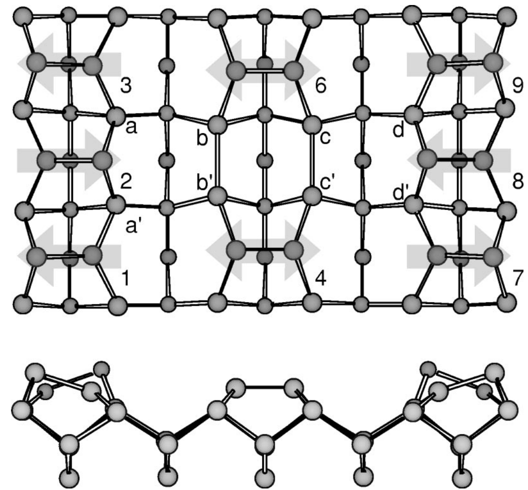

FIG. 3. Optimized structure of the DA_1 model. The cluster model consists of $Si_{75}H_{60}$. Hydrogen atoms are not shown. Arrows indicate buckled directions of dimers defined in Fig. 1. Dimers 4 and 6 were calculated to be symmetric while dimers 1, 2, 3, 7, 8, and 9 were buckled. This structure is the lowest energy arrangement of dimers.

In order to calculate the parameter A, we considered two geometries, DA_1 and DA_2. The optimized structures are shown in Figs. 3 and 4, respectively. As is well known, the rebonding occurs between atoms $b-b'$ $(c-c')$ and, accordingly the induced forces on atoms a and a' (d and d') act to decrease the distance between the atoms $a-a'$ $(d-d')$, leading to that the DA_1 is more favorable than the DA_2.[14,19] The energy difference was calculated to be 25.35 meV, giving $A=6.34$ meV. In other word, the type-A defect plays a role as a pinning center for spins 2 and 8. This effect gives rise to the frustration against the $c(4\times2)$ reconstruction. Thus the observed phenomena may be understood qualitatively by the interplay between these two factors. The new bond lengths $b-b'$ $(c-c')$ were calculated to be 0.283 and 0.284 nm for DA_1 and DA_2, respectively, and the dimers 4 and 6 were symmetric for both structures. The tilted angles of dimers 2 and 8 were calculated to be 20.4° for DA_1

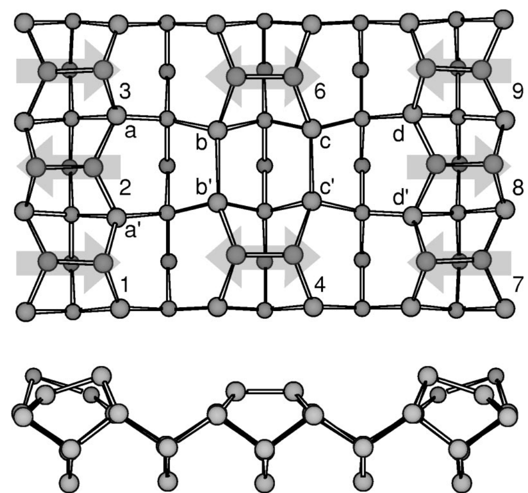

FIG. 4. Optimized structure of the DA_2 model. This structure is the highest energy arrangement of dimers.

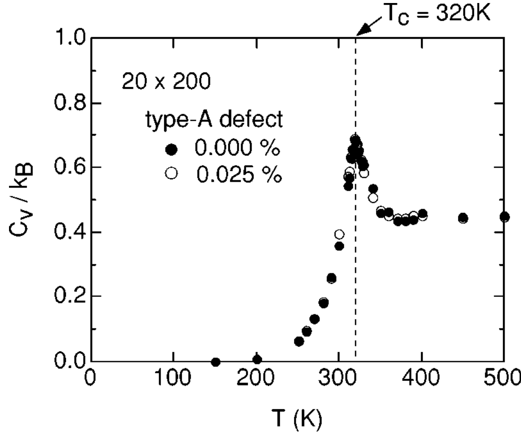

FIG. 5. Specific heat of the Ising model. Results for two cases of defect densities 0.0% (black) and 0.025% (white) are similar. Critical temperature is $T_c^{calc} = 320$ K.

and 18.5° for DA_2, while the calculated angle of the dimer on the clean surface was 20.0°.

In order to check the accuracy of the present calculation, we have also optimized clean surfaces ($Si_{77}H_{60}$), namely, $c(4\times2)$, $p(2\times2)$ and their excited states. The excited states mean that the dimer at the center is buckled opposite direction to that of the ground-state structure, which are labeled $c(4\times2)^*$ and $p(2\times2)^*$, respectively. The calculated total energy differences were $E_{tot}[c(4\times2)^*] - E_{tot}[c(4\times2)] = 193.18$ meV, and $E_{tot}[p(2\times2)^*] - E_{tot}[p(2\times2)] = 195.98$ meV. Then we obtained relations among the interaction parameters V, H, and D as $V = -48.64$ meV and $H - 2D = 0.35$ meV. These values agreed within a few meV with those by band calculations, $V = -51.9$ meV, $H - 2D = -0.6$ meV,[22,23] ensuring the validity of the cluster model. However, it should be noted that no matter how small the value $H - 2D$ may be, its sign has a special meaning. According to the Hamiltonian (1), the value is just the energy difference between the $p(2\times2)$ and $c(4\times2)$, and the positive sign indicates that the former structure is more stable than the latter, contradicting with the observation. Thus, as for the values V, H, and D, we adopted those by the more reliable band calculation.[22,23] On the other hand, the calculated value of A can be used because it is one order of magnitude larger than that of $H - 2D$.

III. PHASE TRANSITION

A. Model and method

We performed a Monte Carlo simulation based on the Ising spin model.[19,22,24] Although dimers 4 and 6 in Figs. 3 and 4 were not tilted, we assigned $\sigma = \pm 1$ for these dimers in the Monte Carlo simulation. We took the lattice size as 20×200. At each temperature, we performed 200 000 MCS for annealing and then averaged next 100 000 MCS. The specific heat of this model was calculated from fluctuation of energy.[25]

B. Monte Carlo simulation

We have calculated specific heat of the Ising model to determine critical temperature T_c^{calc} and clarify an effect of type-A defects on the phase transition. Figure 5 shows the specific heat C_v as a function of temperature T. Specific heats for two cases 0.0 and 0.025% of defect densities coincided with each other. Therefore the phase transition was not affected when the defect density was very low. This is not true for samples with high defect densities. The critical temperature decreased with increasing number of defects and finally the phase transition was not observed at all.[26] The critical temperature at the peak was about $T_c^{calc} = 320$ K, which was consistent with a previously calculated critical temperature of the order-disorder phase transition.[22,23] If we regard the model of Eq. (1) as an anisotropic Ising model, where the interaction parameters are V and $v = H - 2D = -0.6$ meV, the critical temperature T_c satisfies

$$\sinh\left(\frac{2V}{k_B T_c}\right)\sinh\left(\frac{2v}{k_B T_c}\right) = 1, \qquad (2)$$

where k_B is the Boltzmann's constant. The obtained critical temperature is $T_c = 316$ K, which is consistent with the peak temperature of C_v. On the other hand, the experimentally obtained critical temperature is $T_c^{exp} \approx 200$ K,[18] which is about 100 K lower than T_c^{calc}. Using Eq. (2) with the same V, we calculated the value of $H - 2D$ satisfying $T_c = 200$ K. The obtained value was $H - 2D = -0.042$ meV, which was outside of the accuracy limit of the present *ab initio* calculation. This indicates that the reliable theoretical prediction of the T_c is very difficult.

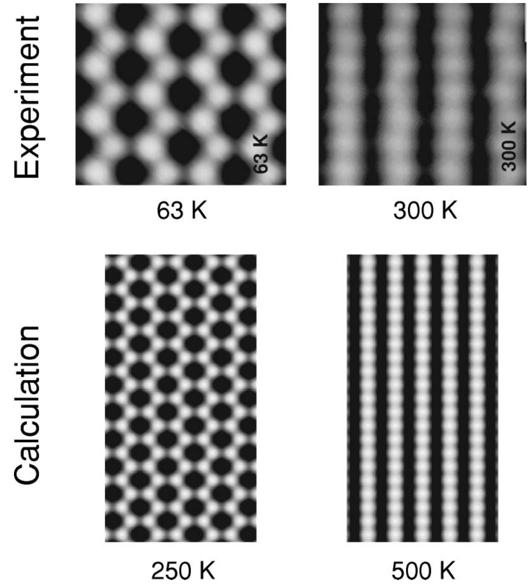

FIG. 6. STM image for the Si(100) clean surface.

C. STM image

STM images for the Si(100) clean surface are shown in Fig. 6 for low and high temperatures. The upper parts of Fig. 6 show our experimental STM images of the Si(100) surface at 63 and 300 K, which were obtained using a constant-current mode of 100 pA at a negative sample voltage of -1.0 V. The experimental details have been described in Ref. 18. At well below T_c, we observed that the buckled dimers were ordered antiferromagnetically, leading to the

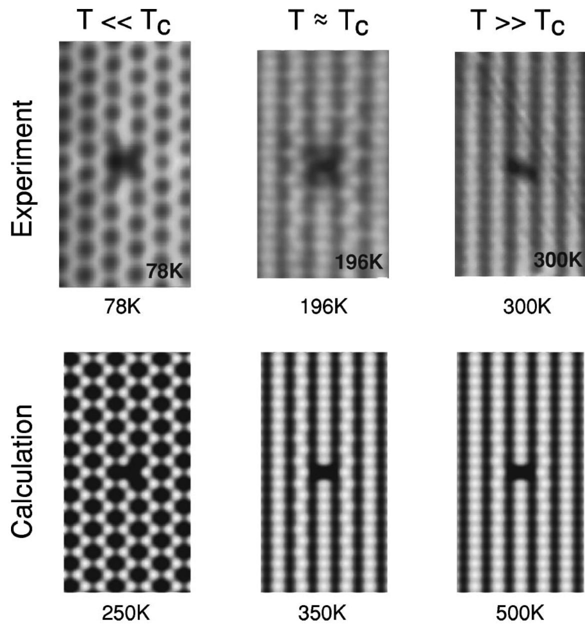

FIG. 7. STM image of the Si(100) surface with single type-*A* defect. Left, middle, and right figures are at $T \ll T_c$, $T \approx T_c$, and $T \gg T_c$, respectively.

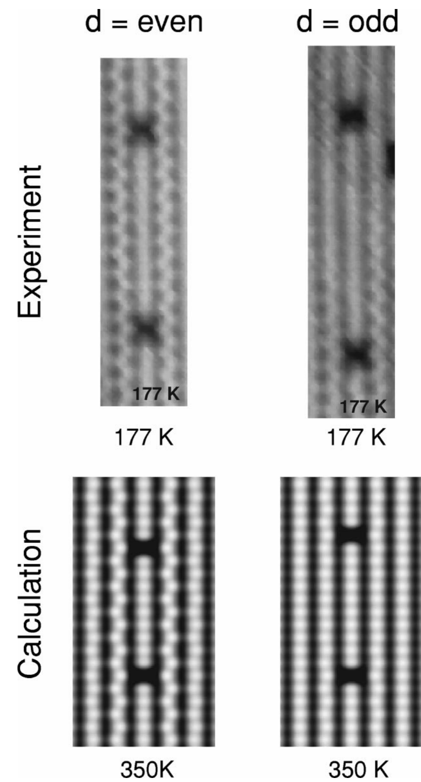

FIG. 8. STM image of the Si(100) surface with two type-*A* defects.

$c(4\times2)$ reconstruction, while the dimers appeared to be symmetric in the room-temperature image. These images were well reproduced by the average values of the spins during the Monte Carlo calculations at 250 and 500 K (see the lower parts of Fig. 6) following the method developed in Ref. 24. These results suggest that the symmetric appearance of the room-temperature image should be generated by the time average of the flip-flop motion of the buckled dimers, and the comparison between the experimental and calculated images enables us to study the dynamical properties during the phase transition.

When the single type-*A* defect was introduced, STM images showed characteristic local structures around the type-*A* defect, which is shown in Fig. 7. When $T \gg T_c$, the STM images were rather symmetric. When $T \approx T_c^{exp}$, a local structure of nanometer size appeared around the type-*A* defect for both experiment and calculation. Below T_c, the $c(4\times2)$ structure appeared and the ''Y''-shaped dark spot was observed in the STM images.

As is clear from the figures, the observed and calculated STM images seem to agree well in all temperature regions. However, there remains a discrepancy which was not explained in the previous paper. The experimental image in the upper middle was taken at 196 K, slightly lower than the experimental critical temperature T_c^{exp}, while the lower middle image was calculated at 350 K, slightly higher than the theoretical critical temperature T_c^{calc}. Below T_c^{calc}, the calculated STM image rapidly changed to the $c(4\times2)$ structure which is shown in the lower left. Moreover, the calculated reconstructed pattern at 350 K faded away as the temperature lowered to T_c^{calc}. These results were confirmed by the careful simulation with greater MCS performed in the present study. Therefore we concluded that the temperature of 196 K should be higher than the T_c^{exp} or, equivalently, the effective T_c^{exp} was lowered by the effect of certain environment surrounding the surface. In fact, it was reported that the critical temperature depends on the environment of the surface.[27]

In case of two type-*A* defects on the Si(100) surface, we observed experimentally that the local structure was enhanced or suppressed depending on the relative location of two defects,[18] as shown in upper part of Fig. 8. The calculated STM images for two cases that the distance between two defects in the same row were *odd* and *even* were shown in lower part of Fig. 8. The images clearly show the enhancement and suppression of the local structures. We also confirmed that the local structures disappeared completely to become $c(4\times2)$ structures below T_c. The agreement between the experiment and the calculation is fairly well.

At the critical temperature, calculated STM images are worth to be mentioned, which is summarized in Fig. 9. As is mentioned above, the STM image of the single defect became symmetric again but for the two defects case the local structure was still enhanced for the *even* distance, and sup-

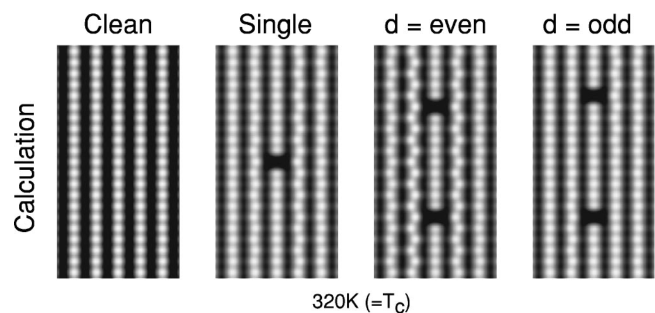

FIG. 9. STM image of the Si(100) surface at 320 K ($=T_c^{calc}$).

pressed for the *odd* distance. Since the various length scale fluctuations become maximum at the critical temperature, the averaged STM images are considered to be sensitive to the defects.

IV. SUMMARY

We have calculated the strain energy caused by the type-*A* defect on the Si(100) surface using the *ab initio* cluster calculation. The obtained strain energy parameter was $A = 6.34$ meV. Then we performed a Monte Carlo simulation for the Ising model regarding the dimers as Ising spins using the interaction parameters obtained by the *ab initio* calculation. A local structure of nanometer size appeared only slightly above T_c in the vicinity of the type-*A* defect. The local structure was enhanced or suppressed depending on the distance between two type-*A* defects above T_c. The calculated STM images reproduced well the experimental ones not only for the images around an isolated type-*A* defect but also for the correlation of the images between two defects. Moreover, our calculated results showed that the structures were rather weakened at T_c except for two defects of *even* distance.

Since the present Monte Carlo simulation can be applied for very large systems, the dynamical behavior of a surface containing such a large number of defects that the phase transition is smeared out, will equally be clarified.

ACKNOWLEDGMENTS

One of the authors (M.O.) would like to thank K. Kato of Joint Research Center for Atom Technology for general discussion about defects on the Si(100) surface. He would also like to thank H. Kawai of Kyushu University for detailed discussion about Monte Carlo simulation techniques. This work was partly supported by New Energy and Industrial Technology Development Organization (NEDO).

*Present address: Joint Research Center for Atom Technology (JRCAT)-Angstrom Technology Partnership (ATP), 1-1-4 Higashi, Tsukuba, Ibaraki 305-0046 Japan.

[1] M. H. White and J. R. Cricchi, IEEE Trans. Electron Devices **ED-19**, 1280 (1972).
[2] T. Sato, Y. Takeishi, H. Hara, and Y. Okamoto, Phys. Rev. B **4**, 1950 (1971).
[3] D. J. Chadi, Phys. Rev. Lett. **43**, 43 (1979).
[4] W. S. Verwoerd, Surf. Sci. **99**, 581 (1980).
[5] M. T. Yin and M. L. Cohen, Phys. Rev. B **24**, 2303 (1981).
[6] Z. Zhu, N. Shima, and M. Tsukada, Phys. Rev. B **40**, 11 868 (1989).
[7] N. Roberts and R. J. Needs, Surf. Sci. **236**, 112 (1990).
[8] A. Ramstad, G. Brocks, and P. J. Kelly, Phys. Rev. B **51**, 14 504 (1995).
[9] T. Tabata, T. Aruga, and Y. Murata, Surf. Sci. **179**, L63 (1987).
[10] M. Kubota and Y. Murata, Phys. Rev. B **49**, 4810 (1994).
[11] R. A. Wolkow, Phys. Rev. Lett. **68**, 2636 (1992).
[12] P. C. Weakliem, G. W. Smith, and E. A. Carter, Surf. Sci. Lett. **232**, L219 (1990).
[13] R. J. Hamers and U. K. Köhler, J. Vac. Sci. Technol. A **7**, 2854 (1989).
[14] K. C. Pandey, in *Proceedings of the 17th International Conference on Physics of Semiconductors*, edited by D. J. Chadi and W. A. Harrison (Springer, New York, 1985), p. 55.
[15] H. Tochihara, T. Amakusa, and M. Iwatsuki, Phys. Rev. B **50**, R12 262 (1994).
[16] T. Uda and K. Terakura, Phys. Rev. B **53**, 6999 (1996).
[17] T. Miyazaki, T. Uda, and K. Terakura, Phys. Rev. Lett. **84**, 4128 (2000).
[18] T. Yokoyama and K. Takayanagi, Phys. Rev. B **56**, 10 483 (1997).
[19] M. Okamoto, T. Yokoyama, and K. Takayanagi, Surf. Sci. **402-404**, 851 (1998).
[20] J. Ihm, D. H. Lee, J. D. Joannopoulos, and J. J. Xiong, Phys. Rev. Lett. **51**, 1872 (1983).
[21] S. J. Vosko, L. Wilk, and M. Nusair, Can. J. Phys. **58**, 1200 (1980).
[22] K. Inoue, Y. Morikawa, K. Terakura, and M. Nakayama, Phys. Rev. B **49**, R14 774 (1994).
[23] K. Terakura, T. Yamasaki, and Y. Morikawa, Phase Transit. **53**, 143 (1995).
[24] Y. Nakamura, H. Kawai, and M. Nakayama, Phys. Rev. B **52**, 8231 (1995).
[25] J. J. Binney, N. J. Dowrick, A. J. Fisher, and M. E. J. Newman, *The Theory of Critical Phenomena* (Oxford University Press, New York, 1992), p. 44.
[26] T. Yokoyama, M. Okamoto, and K. Takayanagi, in *The Electron: Proceeding of the International Centennial Symposium on the Electron*, edited by A. Kirkland and P. D. Brown (IOM Communications Ltd., London, 1998), pp. 639–644.
[27] T. Yokoyama and K. Takayanagi, Phys. Rev. B **57**, R4226 (1998).